Unsteady, Separated Flow Behind an Oscillating, Two-Dimensional Spoiler

Curtis F. Nelson,* Dennis J. Koga,† and John K. Eaton‡
Stanford University, Stanford, California

Unsteady, separated flow produced downstream of a two-dimensional lifting spoiler was examined experimentally using phase-averaged laser-Doppler anemometer and surface pressure measurements. Special emphasis was placed on measuring the unsteady, reversing flow just behind the spoiler. Sinusoidal spoiler oscillations with reduced frequencies in the range 0.025–0.06 were used to create unsteady vortices in the flow, and pitch-and-hold spoiler motions were used to investigate the evolution of the unsteady vortex into a steady separation. Phase-angled vorticity was calculated from the velocity data and the development of the unsteady vortex formed downstream of the spoiler was analyzed. The dominant mechanism of vorticity transport is found to be convective.

Nomenclature

c_p = pressure coefficient, $(P - P_{ref})/(\rho U_{ref}^2/2)$
f = frequency of the spoiler oscillation cycle, Hz
k = reduced frequency based on spoiler chord, $= fL/U_{ref}$
L = spoiler chord length, = 25.4 mm
P = static pressure on the wind-tunnel bottom wall
P_{ref} = reference (tunnel centerline) static pressure
t = time ($t = 0$ when the spoiler is flush with the tunnel bottom and just starting to rise)
U_{ref} = reference (tunnel centerline) velocity, = 5 m/s
u, u_1 = velocity component in the x direction
v, u_2 = velocity component in the y direction
x, x_1 = streamwise distance from the spoiler rotation axis (see Fig. 2)
y, x_2 = vertical distance from the tunnel bottom wall (see Fig. 2)
z, x_3 = spanwise distance from the tunnel centerline
Γ = circulation
δR = uncertainty in the result R (95% confidence)
θ = spoiler rotation angle (see Fig. 2)
ϕ = phase in the oscillatory spoiler cycle: $\phi = 0$ deg occurs at the point $\theta = 45$ deg when the spoiler is rising from the wall (see Fig. 2)
ρ = density
ν = kinematic viscosity
ω_3 = spanwise vorticity, $= \partial v/\partial x - \partial u/\partial y$
$\overline{(\,)}$ = phase-averaged component; average of a quantity when taken at the same point, or phase, in each cycle of a record of many cycles
$(\,)'$ = turbulent component

Introduction

THE flow behind a two-dimensional lifting spoiler serves as a simple model of more general unsteady, separated flows and also has practical application in its own right. It has been recognized that large vortical structures are the dominant features in these flows and that the unsteady effects produced by these structures can be either beneficial or detrimental to overall device performance.[1-4] For example, the initial flow structure that rolls up behind the spoiler creates a strong spanwise vortex with a corresponding low pressure on the surface which causes a substantial short-term lift force. If the spoiler remains extended, a steady separation is formed as the vortex either sheds or decays, and the lift augmentation is lost. Coherent strutures in the separated shear layer formed from the trailing edge of the spoiler, although not strong enough to cause lift augmentation, can cause substantial buffeting. Understanding and manipulation of the unsteady flow structures would enable one to take advantage of the beneficial effects while mitigating the detrimental effects.

Previous researchers have investigated related unsteady flows generated by moving control surfaces, usually in an attempt to dynamically reattach an otherwise separated flow. These studies have typically used flow visualization, surface pressures, and hot-wire anemometry as the means of acquiring the data. Francis et al.[1] studied the unsteady flowfield generated by the oscillation of a fence-type spoiler on an airfoil using a hot-wire anemometer. Consigny et al.[5] studied the effects of different motions of a hinged spoiler on the pressure distribution on a supercritical airfoil; this work was later extended by adding an unsteady, trailing-edge flap.[6] Flow visualization and hot-wire measurements were used by Viets et al.[7] to study the flowfield generated by a rotor mounted on a wall, and by Huyer and Luttges[8] to study an airfoil with a periodically deformable leading edge in order to promote reattachment past the static stall angle of attack.

Previous work on the lifting-spoiler flow by Koga[9] and Reisenthel et al.[3] used smoke-wire flow visualization combined with surface pressure and hot-wire measurements to identify the frequency range for the production of large coherent vortices. They also studied the utilization of vortices produced by the lifting spoiler in order to reduce the reattachment length of steady separation for various configurations. This work and that of Nagib et al.[10] have shown that the reduced frequency is the fundamental parameter for characterizing these unsteady flowfields. Using surface pressure measurements, Ahmed and Hancock[11] investigated the time development of the separated region for a rapidly rising spoiler and found it to be a function only of the ratio of spoiler rise time

Received Nov. 14, 1988; presented as Paper 89-0288 at the AIAA 27th Aerospace Sciences Meeting, Reno, NV, Jan. 9-12, 1989; revision received June 30, 1989.

*Research Assistant. Student Member AIAA.
†Senior Research Associate. Member AIAA.
‡Associate Professor and Associate Chairman. Member AIAA.

to spoiler chord convection time. Computational studies of the lifting-spoiler flow have used both inviscid flow models, such as the discrete-vortex method,[12,13] and unsteady Navier-Stokes computations[14] to calculate flows behind lifting and oscillating spoilers. The inviscid methods work well if the spoiler descends before the vortex begins to diffuse substantially.

The objective of the present study was to obtain detailed velocity measurements using a laser-Doppler anemometer (LDA) in the unsteady and separated flow region behind an oscillating spoiler. Special emphasis was placed on the unsteady, reversing flow just behind the spoiler since reliable hot-wire measurements are not possible in this region. Both sinusoidal spoiler waveforms and a waveform in which the spoiler pitches up rapidly then holds in the extended position have been examined. The velocity measurements are used to increase the understanding of the basic mechanisms operative in unsteady, separated flows.

Experimental Technique

The experiments were performed in a low-speed, 150 mm × 450 mm, open-circuit wind tunnel documented in earlier backward-facing step flow experiments.[15] The test section was modified to eliminate the step and install the flush-mounted spoiler. The approach flow is tripped on all four tunnel walls and the boundary layers are allowed to develop over a 3.5-m length. The sidewall boundary layers are removed approximately 27 spoiler chord lengths upstream of the spoiler to maintain a two-dimensional approach flow. At the nominal centerline velocity of 5 m/s, the Reynolds number based on spoiler chord is 8200, and the boundary-layer momentum thickness Reynolds number is 1600.

The two-dimensional spoiler is located on the bottom wall of the tunnel and spans the test section as shown in Fig. 1. The spoiler aspect ratio (span/chord) is 18 to insure two-dimensionality of the separated region.[16] The spoiler is actuated by a computer-controlled servo system driving a PMI Motion Technologies printed-circuit motor directly connected to the spoiler shaft, and is free to oscillate from a position flush with the bottom surface of the tunnel surface of the tunnel ($\theta = 0$ deg) to a position perpendicular to the bottom wall ($\theta = 90$ deg). The control waveform is specified by loading appropriate position information into computer memory and sending the signal out through a digital-to-analog converter to the servo system. Spoiler position and velocity feedback were provided by a rotary variable differential transformer (RVDT) and tachometer, both mounted directly to the spoiler drive shaft.

The flowfield in the periodically separated region downstream of the oscillating spoiler was examined using smoke-wire flow visualization, surface pressure measurements, and laser anemometry. Flow visualization showed that the flow structure was repeatable from cycle to cycle, thus all measurements were phase-conditioned on the phase of the spoiler motion. Pressure measurements were made using a Validyne CD15 carrier/demodulator and a Validyne DP45-16 pressure transducer connected differentially between the tunnel floor and the freestream static pressure.

The LDA measurements were made with a single-component, Bragg-shifted, forward-scattering system using a TSI

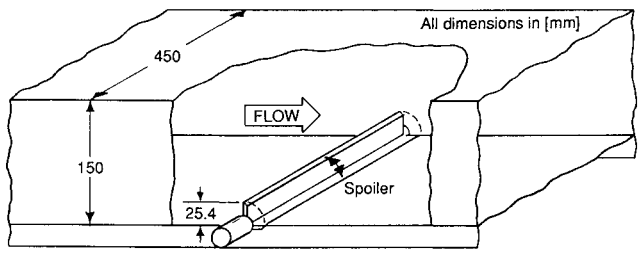

Fig. 1 Schematic of wind tunnel.

Table 1 Vorticity and vorticity uncertainty

Flap motion	Vorticity $\bar{\omega}_3 L/U_{ref}$ Minimum	Mean	Maximum	Vorticity uncertainty $\delta\bar{\omega}_3 L/U_{ref}$ Mean	Maximum
5 hz sinusoidal	−16.18	−0.24	8.89	0.07	4.79
8 hz sinusoidal	−20.10	−0.30	5.73	0.05	3.97
12 hz sinusoidal	−10.32	−0.24	2.80	0.04	0.97
Pitch-and-hold	−16.81	−0.35	7.76	0.06	3.09

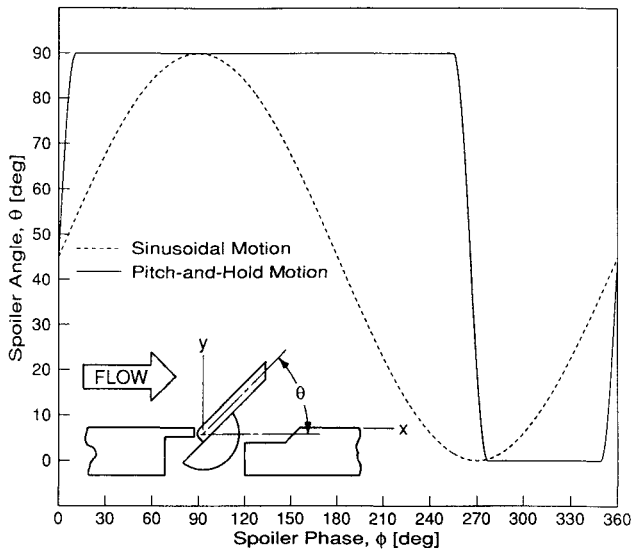

Fig. 2 Spoiler waveforms.

Model 1980 counter processor to measure the Doppler frequency. The beams were rotated to acquire either the u or v component of the velocity. Condensed mineral oil droplets were supplied upstream of the wind-tunnel blower for LDA seeding. Special handling of the velocity data was required since the seed particles arrive at the LDA measurement volume at random phases of the spoiler cyle. Spoiler phase information was acquired simultaneously with each velocity sample. The data was then placed into phase bins and the velocity averaged over all of the samples in a given bin. Typically 50,000 samples of each velocity component were acquired at each measurement point and phase-averaged into 36 bins. This allowed good resolution of the unsteady flow while keeping the number of samples per bin large enough for good statistics. Using a larger number of phase bins does not effect the results substantially. The acquisition required a minimum of 300 spoiler cycles for the sinusoidal spoiler motions and 100 cycles for the pitch-and-hold motion. A field of data consists of two components of velocity at each of 74 to 161 measurement points.

The phase-averaged vorticity was calculated by fitting the two-dimensional velocity field for each phase bin with natural cubic splines in both directions and analytically differentiating the splines. To insure that the splines do not introduce spurious oscillations or peaks, estimates of the uncertainty in the vorticity values were calculated. Uncertainty in the measurement location and uncertainty due to the finite number of acquired samples[17] were propagated numerically[18] through the splines into the velocity derivatives and vorticity. Uncertainty due to LDA resolution is assumed to be small and was not 4 included.

Table 1 gives statistics on both the vorticity and the vorticity uncertainty for the four spoiler motions that were investigated. The tabulated values were calculated using data from every point in the field over every phase bin. The uncertainties are small relative to the vorticity in the unsteady vortex, indi-

cating that the spline interpolation does not cause the vorticity to oscillate wildly due to the presence of errors. The uncertainties are smallest for the $k = 0.06$ case due to its wider data spacing relative to the other cases; this also causes the reduction in the peak vorticity levels for this case.

Results and Discussion

The data consist of phase-averaged velocity and vorticity fields along the centerline plane of the wind tunnel and the corresponding phase-averaged surface pressures on the bottom wall of the tunnel for the following four cases, all at a nominal centerline velocity of 5 m/s:

1) 5-Hz sinusoidal oscillation ($k = 0.025$) from $\theta = 0$ tunnel to 90 deg.

2) 8-Hz sinusoidal oscillation ($k = 0.04$) from $\theta = 0$ to 90 deg.

3) 12-Hz sinusoidal oscillation ($k = 0.06$) from $\theta = 10$ to 80 deg (no wider range of angles was possible due to the frequency response of the spoiler drive mechanism).

4) Pitch-and-hold motion (effective $k = 0.04$) from $\theta = 0$ deg to 90 deg.

Figure 2 shows the relationship between spoiler angle and spoiler phase for the two types of spoiler waveforms investigated. These reduced frequencies are rather low as the maximum speed of the spoiler tip is only $0.23U_{ref}$ for the cases investigated. The pitch-and-hold motion is actually a 1-Hz cycle (360 deg spoiler phase = 1 s) that starts and ends as 8-Hz half-sinusoids (effective $k = 0.04$) with the spoiler holding for 0.675 s at its maximum extension from the tunnel floor. After the spoiler returns to the wall, it remains flush with the bottom wall of the tunnel for 0.2 s in order for the flow to re-establish itself before the start of the next cycle.

Unsteady Velocity and Vorticity

Figures 3-6 show acquired velocity vectors and the corresponding vorticity contours from six of the phase bins that make up the entire cycle for each of the four cases. The direction and envelope of spoiler motion are shown along with legends giving the phase and dimensionless time for each phase bin. These figures clearly show that the flow is dominated by the presence of a large, unsteady vortex.

As the spoiler rises away from the wall, a strong vortex is formed and negative velocities with magnitudes larger than U_{ref} are observed near the wall immediately downstream of the spoiler. The vortex grows until the spoiler reaches its maximum extension away from the wall. When the spoiler begins to move back toward the wall, the vortex is released and convects downstream. As the vortex convects, its peak vorticity decays rapidly due to viscous and turbulent diffusion. As shown in Figs. 3-5, the size of the vortical region formed behind the spoiler decreases as the reduced frequency is increased. This follows from the fact that there is more time for boundary-layer vorticity both to accumulate and diffuse in the separated vortex as the spoiler frequency is reduced. At the low reduced frequencies, the vortex looks much like a quasi-steady separated region and a large shear layer is formed starting at the trailing edge of the spoiler. As the reduced frequency is increased, the size of this shear layer decreases and the unsteady vortex becomes more coherent. The presence of the strong, coherent vortex induces a weak region of secondary positive vorticity upstream of itself as it convects downstream. Some of the loss of coherence at low reduced frequencies is caused by smearing of the vortex due to the nonzero width of the phase bins.

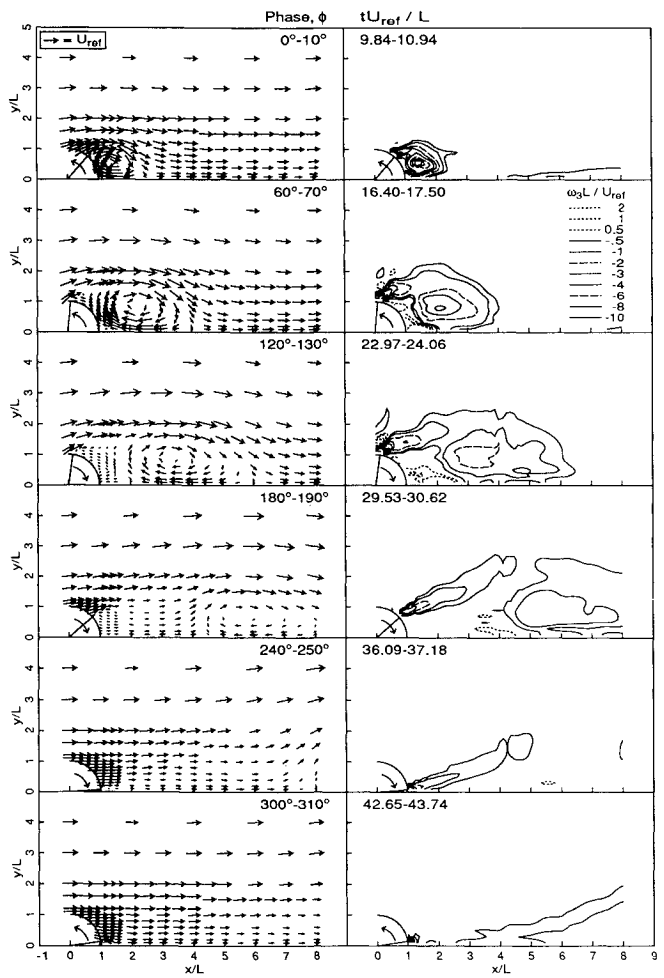

Fig. 3 Unsteady flowfield for 5-Hz sinusoidal spoiler motion ($k = 0.025$).

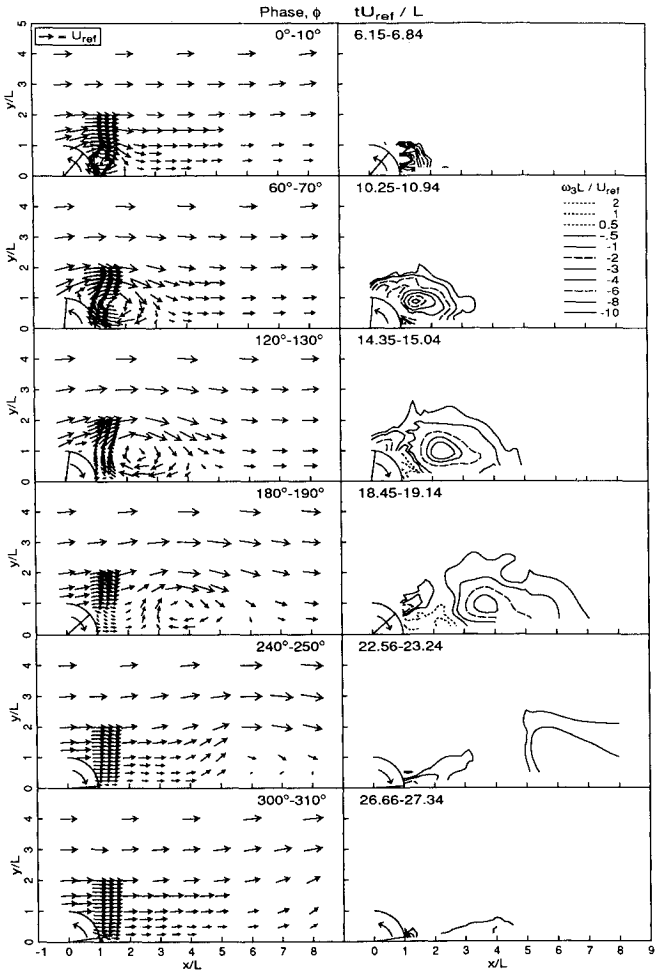

Fig. 4 Unsteady flowfield for 8-Hz sinusoidal spoiler motion ($k = 0.04$).

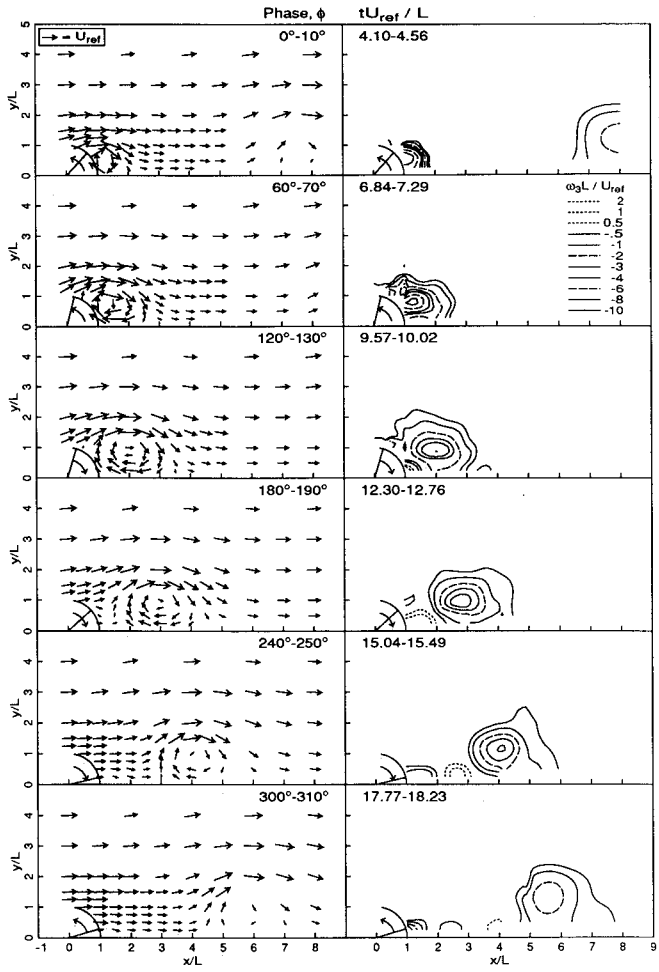

Fig. 5 Unsteady flowfield for 12-Hz sinusoidal spoiler motion ($k = 0.06$).

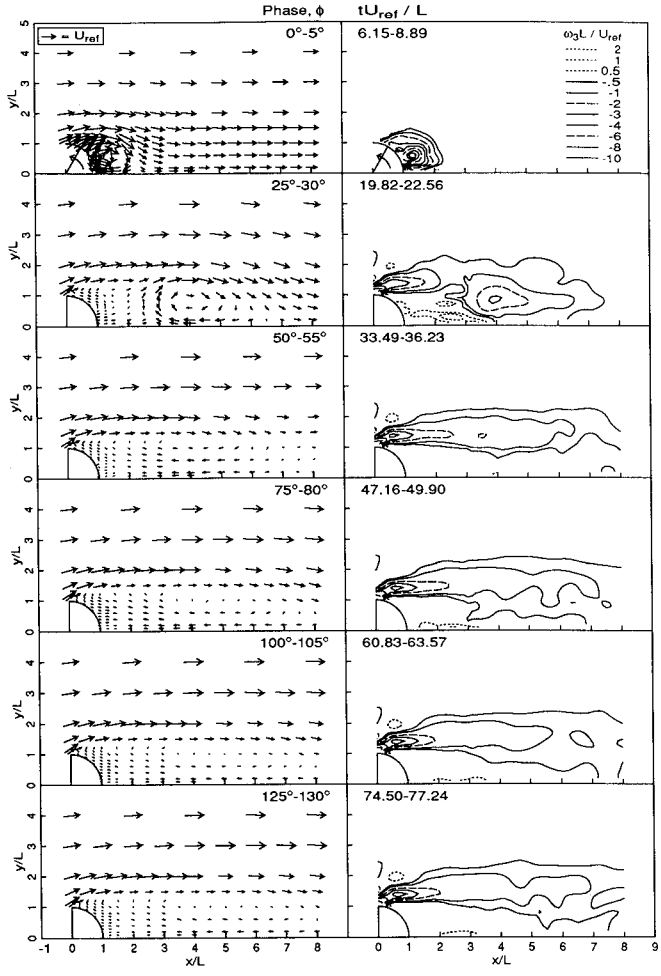

Fig. 6 Unsteady flowfield for pitch-and-hold spoiler motion.

The pitch-and-hold waveform was investigated as a method of examining the unsteady vortex evolving into a steady separation. Figure 6 shows the velocity vectors and vorticity contours for this flowfield. As the spoiler rises, a strong unsteady vortex is formed, much like the 8-Hz sinusoidal case shown in Fig. 4. However, since the spoiler holds when it reaches its maximum extension, the vortex is not cleanly carried away by the freestream fluid. Instead, a large separated region forms as boundary-layer vorticity is carried over the spoiler by the mean flow. The vorticity contours in Fig. 6 show the formation of a large shear layer at the trailing edge of the spoiler. The unsteady behavior of the vortex was examined in more detail using 72 phase bins. During the time in which the spoiler rises ($\theta = -11.25$ to 11.25 deg), the spoiler motion and the flowfield are exactly the same as the $k = 0.04$ sinusoidal case. When the spoiler holds at its maximum extension, the vortex begins to convect downstream while a shear layer forms at the spoiler trailing edge. By the 45–50 deg phase bin, the vortex has convected out of the data window, the flow behind the spoiler is stagnant, and a shear layer has formed from the spoiler trailing edge. However, in the range of phases from 50–65 deg the fluid near the wall in the separated region surges toward the spoiler and the shear layer dips toward the wall. The flow then slowly adjusts until a steady separated region has been established by 120-deg phase. The steady reattachment point is not seen in Fig. 6 as it occurs at $x/L \approx 15$.[11] It should be noted that the "steady" separation contains large unsteadiness, but these velocity fluctuations are not phase correlated.

Unsteady Pressure

Figures 7–9 show the unsteady pressure measured on the bottom of the tunnel for the sinusoidal spoiler cycles corresponding to the velocity fields in Figs. 3–5. In each case, the data show a well-defined negative pressure peak that convects downstream. This is a clear signature of the vortex observed in the detailed velocity measurements, suggesting that wall pressure data may be sufficient to track the vortices.

Pressure data for the pitch-and-hold spoiler motion are shown in Fig. 10. An unsteady vortex is formed as the spoiler rises from the bottom wall of the tunnel; however, as the vortex convects downstream a low-pressure, steady separated region is left behind, in agreement with the results shown in Fig. 6. The pressure overshoot that occurs between the large negative peak of the unsteady vortex and the flat region of the steady separation corresponds to the phase range in which the surge of backflow occurred. Figure 10 shows that the flowfield reaches its steady state much faster when the spoiler returns to the wall than when the spoiler is rising. For the rising spoiler, the flowfield reaches its steady state slowly as an equilibrium must be reached between convection into and entrainment out of the separated region. When the spoiler returns to the wall, the steady state is quickly attained as the separation is simply flushed downstream by the freestream flow.

Vortex Development

The position and circulation of the unsteady vortex was calculated as a function of phase for sinusoidal spoiler motions in order to quantify the development of the vortex. This

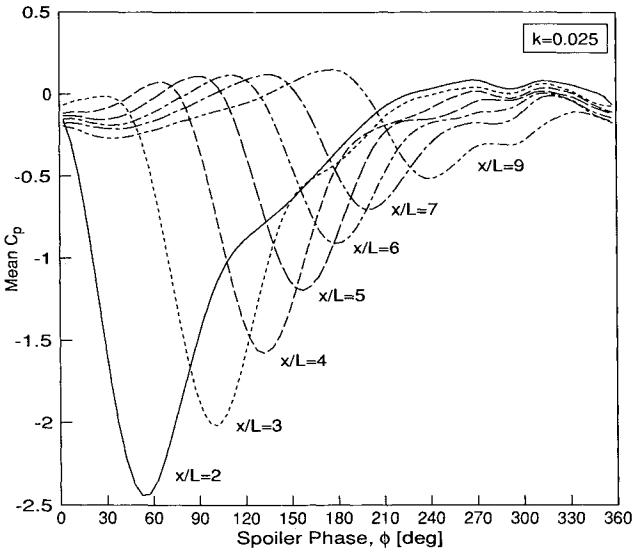

Fig. 7 Unsteady pressure for 5-Hz sinusoidal spoiler motion ($k = 0.025$).

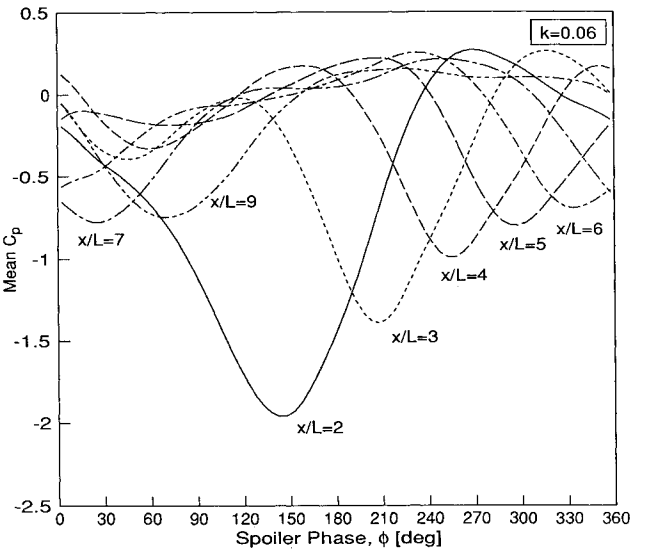

Fig. 9 Unsteady pressure for 12-Hz sinusoidal spoiler motion ($k = 0.06$).

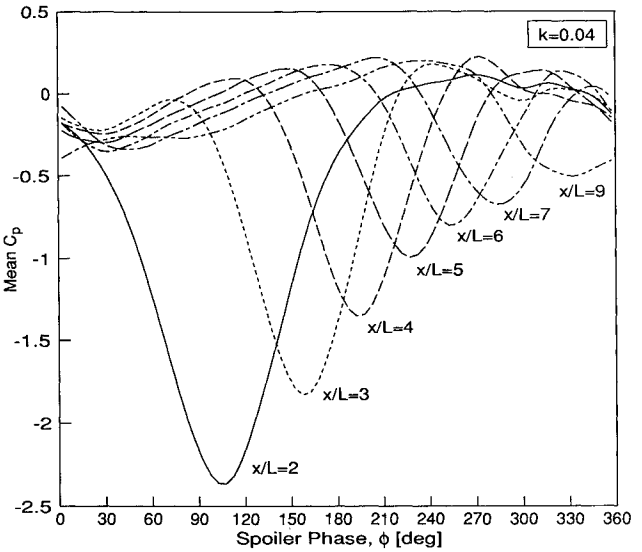

Fig. 8 Unsteady pressure for 8-Hz sinusoidal spoiler motion ($k = 0.04$).

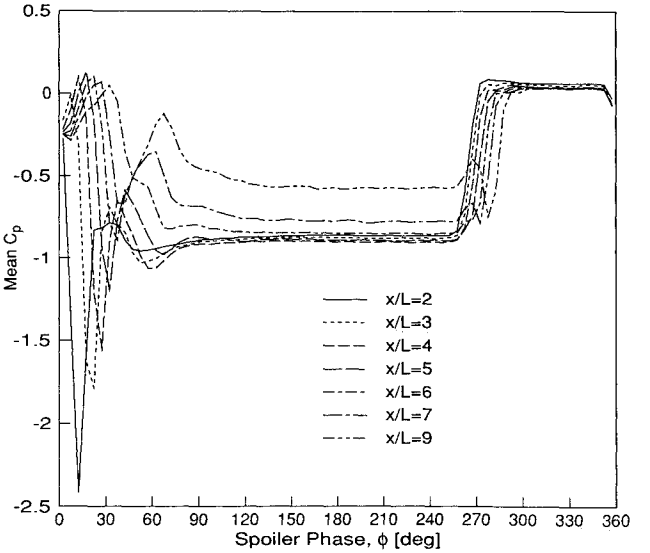

Fig. 10 Unsteady pressure for pitch-and-hold motion.

was done by assuming that the vortex consisted of the fluid inside a given vorticity contour and integrating the vorticity over all points enclosed by the contour. The contour level $\tilde{\omega}_3 L/U_{\text{ref}} = -1.27$ was chosen as it includes all of the fluid which obviously belongs to the vortex, while excluding low-level vorticity and noise in the background. The results for the $k = 0.04$ and 0.06 cases are plotted vs dimensionless time in Fig. 11, starting when the spoiler is flush with the tunnel bottom (i.e., starting at $\phi = 270$ deg for sinusoidal oscillations). The $k = 0.025$ case is not shown as a large, elongated separated region is formed at this low reduced frequency, leaving no clearly defined vortex over which to integrate (see Fig. 3).

Figure 11a shows the circulation contained in the vortex. The peak circulation is larger for the $k = 0.04$ case since the slower spoiler motion allows more time for the boundary-layer vorticity to be rolled-up into the vortex. However, due to the fact that there are more vortices formed per unit time for the $k = 0.06$ case (i.e., there are 12 vortices formed/s vs 8/s for the $k = 0.04$ case), the sum of the circulation in the vortices formed per unit time is approximately equal for the two cases. During the portion of the cycle in which the spoiler is moving away from the wall, the circulation in the vortex increases due to the influx of boundary-layer vorticity flowing over the spoiler. Once the spoiler begins to move back towards the wall, the circulation decreases as the vortex convects downstream and vorticity diffuses out of the vortex. The circulation finally falls rapidly to zero as the vortex convects out of the window in which data was acquired.

From the slope of the curves in Fig. 11b, the vortex reaches a limiting velocity of about 60% of the centerline velocity for both cases; however, the vortex in the higher reduced frequency case is released from the spoiler at an earlier time due to the increased spoiler frequency. Using potential flow ideas,[19] the vortex moves downstream slower than the centerline velocity due to induced upstream motion caused by its image vortex in the wall.

Figure 11c shows the height of the vortex centroid above the bottom tunnel wall. The vortex follows the sinusoidal motion of the spoiler to a height of $y/L \approx 1$ and then remains at approximately the same height for the rest of the cycle. The curves become noisy at later times as the vortex begins to convect out of the region where data was acquired, making it difficult to define where the center of the vortex is located.

Vorticity Transport

To take a closer look at the transport of vorticity in this flow, the vorticity fluxes have been calculated through control volumes located downstream of the spoiler. Utilizing tensor notation with Einstein's summation convention,[20] the vorticity equation for an incompressible Newtonian fluid of constant viscosity can be written as

$$\frac{\partial \omega_i}{\partial t} + \frac{\partial (u_k \omega_i)}{\partial x_k} = \frac{\partial (\omega_k u_i)}{\partial x_k} + \nu \frac{\partial^2 \omega_i}{\partial x_k \partial x_k} \tag{1}$$

The time-dependent velocity and vorticity terms can be decomposed into a phase-averaged mean term and a turbulent term. By phase-averaging the resulting equation, the phase-averaged mean vorticity transport equation becomes

$$\frac{\partial \bar{\omega}_i}{\partial t} + \frac{\partial (\bar{u}_k \bar{\omega}_i)}{\partial x_k} + \frac{\partial (\overline{u_k' \omega_i'})}{\partial x_k} = \frac{\partial (\bar{\omega}_k \bar{u}_i)}{\partial x_k} + \frac{\partial (\overline{\omega_k' u_i'})}{\partial x_k} + \nu \frac{\partial^2 \bar{\omega}_i}{\partial x_k \partial x_k} \tag{2}$$

After assuming no gradients or mean flow in the spanwise direction ($\partial/\partial x_3 = 0$ and $\bar{u}_3 = 0$), the phase-averaged mean spanwise vorticity equation can be rewritten in flux form[19] as

$$\frac{\partial \bar{\omega}_3}{\partial t} + \frac{\partial \bar{F}_k}{\partial x_k} = 0 \tag{3}$$

$$\bar{F}_k = \bar{u}_k \bar{\omega}_3 - \nu \frac{\partial \bar{\omega}_3}{\partial x_k} + \overline{\omega_3' u_k'} - \overline{\omega_k' u_3'} \tag{4}$$

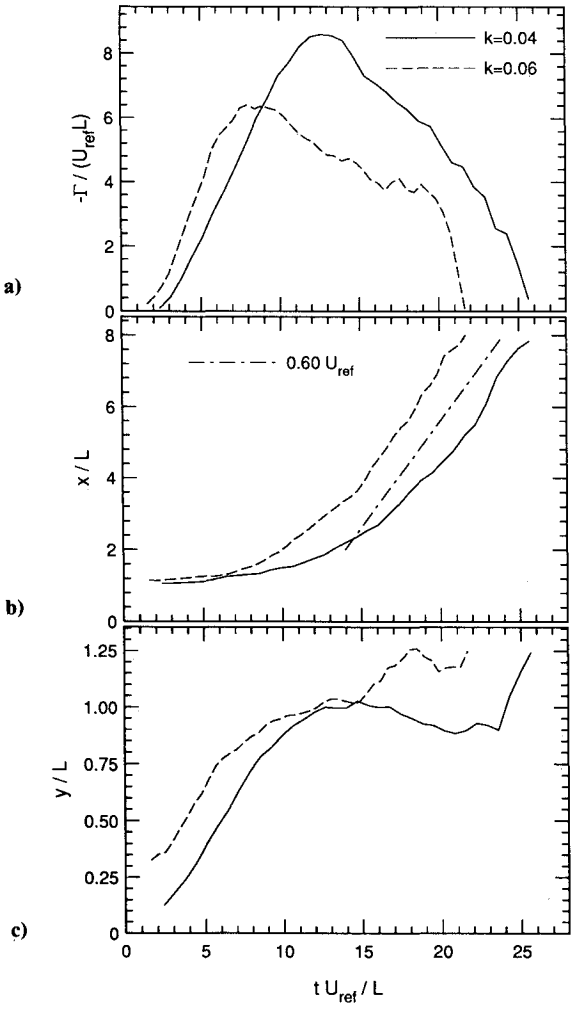

Fig. 11 Unsteady vortex development.

where $\bar{F}_1$ and $\bar{F}_2$ are the phase-averaged mean vorticity fluxes in the x and y directions. When the turbulent vorticity terms are expanded into derivatives of turbulent velocities, $\bar{F}_1$ and $\bar{F}_2$ are given by[21]

$$\bar{F}_1 = \bar{u}_1 \bar{\omega}_3 - \nu \frac{\partial \bar{\omega}_3}{\partial x_1} + \frac{\partial}{\partial x_1}(\overline{u_1' u_2'}) + \frac{\partial}{\partial x_2}\left(-\frac{\overline{u_1' u_1'}}{2} + \frac{\overline{u_2' u_2'}}{2} - \frac{\overline{u_3' u_3'}}{2} \right) \tag{5}$$

$$\bar{F}_2 = \bar{u}_2 \bar{\omega}_3 - \nu \frac{\partial \bar{\omega}_3}{\partial x_2} + \frac{\partial}{\partial x_1}\left(-\frac{\overline{u_1' u_1'}}{2} + \frac{\overline{u_2' u_2'}}{2} + \frac{\overline{u_3' u_3'}}{2} \right) - \frac{\partial}{\partial x_2}(\overline{u_1' u_2'}) \tag{6}$$

The various terms in the fluxes represent vorticity transport by convection, viscous diffusion, shear-stress gradient, and normal-stress gradient. Note that under our assumption of two-dimensional flow in the mean, there is no vorticity transport by vortex stretching. The normal stress in the z direction and the shear-stress terms were not measured; however some idea of their magnitude can be inferred by the amount by which this equation does not balance. Experimental error and three-dimensionality will also contribute to the imbalance.

In order to avoid using second derivatives of the acquired velocity data, the vorticity flux equation was integrated in space over a control volume in the flowfield to give the vorticity flows through the surfaces of the control volume. This integration was carried out for all four cases and the results are shown in Figs. 12–15. The inset in each figure shows the control volume that was used, where each surface is shown in the same line style used to plot the flow across that surface. The vorticity flow in the positive x or y direction through each of the four surfaces defining the control volume is shown as a function of spoiler phase, with the net vorticity flow into the control volume plotted as a solid line. Since the dominant vorticity in this flow is negative, a flow in the positive coordinate direction will have a negative sign. The net flow should sum to zero over the entire cycle as this is equivalent to integrating the vorticity flux equation in time over a complete spoiler cycle, and there can be no net increase or decrease of vorticity in the control volume since the flow is periodic.

In all cases, there is a large flow of vorticity into the control volume through the upstream control volume surface and a

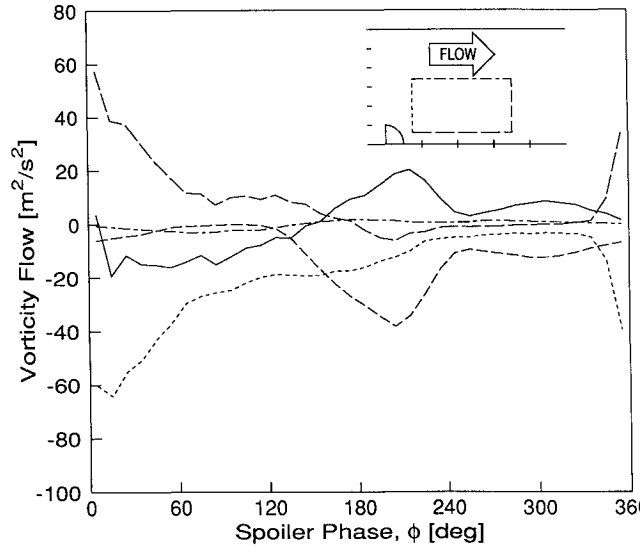

Fig. 12 Unsteady vorticity flow for 5-Hz sinusoidal spoiler motion ($k = 0.025$).

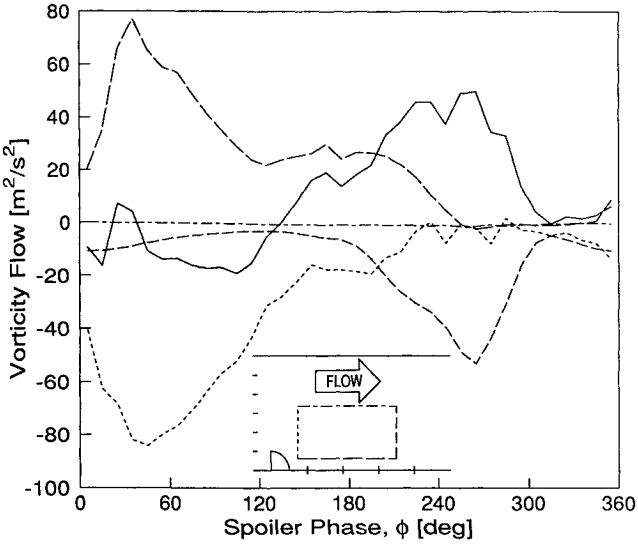

Fig. 13 Unsteady vorticity flow for 8-Hz sinusoidal spoiler motion (k = 0.04).

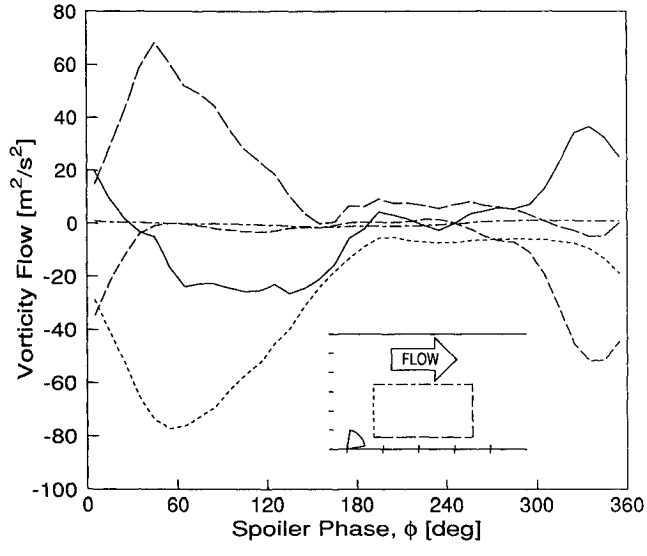

Fig. 14 Unsteady vorticity flow for 12-Hz sinusoidal spoiler motion (k = 0.06).

large flow of vorticity out the bottom surface while the spoiler is rising. This is consistent with the fact that vorticity will be carried in through the upstream surface and out the bottom surface of the control volume as the vortex rolls up behind the spoiler. During this part of the cycle, the net flow shows an overall inflow of vorticity since the vortex is growing into the control volume. When the vortex convects downstream, its streamwise extent is entirely contained within the control volume and thus the flows through the upstream and downstream surfaces of the control volume are small. The flow through the bottom surface is also small as the upstream side of the vortex produces an inflow and its downstream edge produces an outflow of vorticity through the bottom surface which effectively cancel one another. When the vortex convects out the downstream surface of the control volume there is a large net outward flow of vorticity. The flow of vorticity out the upper surface of the control volume during the cycle is negligible as the surface was located well out in the freestream. Because the vortex is much more coherent for the higher reduced frequency (k = 0.06) case, the flow terms shown in Fig. 14 are essentially zero for spoiler phases from 170–300 deg when the vortex is contained entirely within the control volume. The shear layers that are formed from the spoiler at the lower

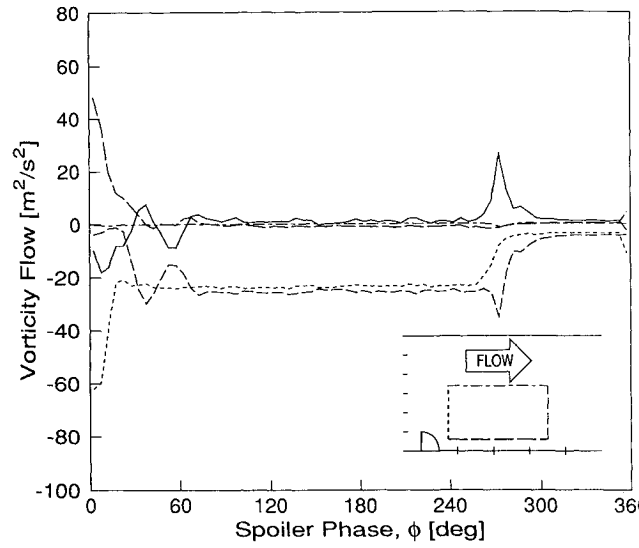

Fig. 15 Unsteady vorticity flow for pitch-and-flow spoiler motion.

reduced frequencies keep the flow through the upstream surface of the control volume from going to zero, even when the unsteady vortex is entirely within the control volume. Comparison between Figs. 3–5 and Figs. 12–14 show excellent agreement as to when the vortex enters and leaves the control volume.

Figure 15 shows the same results for the pitch-and-hold case. Since a steady separation is formed, the vorticity flow into the upstream surface is equal to the flow out of the downstream surface for most of the cycle. A net change in the vorticity in the control volume occurs only when the spoiler is rising or falling. For example, from 254.25 to 276.75-deg phase the spoiler goes from being perpendicular to flush with the wall. The flow of vorticity into the upstream surface stops at about 280-deg phase and it stops flowing out of the downstream surface about 10 deg later in phase which is approximately the time it takes for the freestream to traverse the length of the control volume, carrying away the vortical fluid that was contained in the separated region.

Convection is the dominant term in the vorticity transport equation. For all cases, the measured normal-stress gradient terms are usually at least two orders of magnitude smaller and the viscous diffusion term three orders of magnitude smaller. The sum of the net flow over the entire cycle for the k = 0.04 sinusoidal case is equal to about 30% of the flow through the upstream surface of the control volume instead of summing to zero. However, for all of the other cases, the net flow sums to well under 5% of the flow through the upstream surface which seems to indicate that the unmeasured three-dimensional and shear-stress gradient terms are not very large. The fact that the flows are dominated by the convective term is the reason that inviscid models give good results when modeling this flow. Note that even though the viscous and turbulent diffusion terms are small compared to the convective term for the overall transport of vorticity, these terms govern the growth of the vortex size and the time behavior of the peak vorticity.

Conclusions

Detailed phase-averaged measurements of unsteady velocity and pressure have been obtained in the unsteady, separated flow downstream of an oscillating spoiler. Over the range of reduced frequencies examined, the separation varies from a rather ill-defined vortical region to one with discrete, tightly wound vortices. The phase-conditioned velocity measurements have provided quantitative estimates of vortex size, position, and strength in an unsteady separated flow. The vortex circulation decreases as the reduced frequency of the

spoiler motion is increased; however, the circulation per unit time remains relatively constant. For the range of reduced frequencies examined, convection of vorticity is the dominant term in the vorticity transport equation, while transport by turbulent stress gradients and viscous diffusion is several orders of magnitude smaller.

Acknowledgment

This work is supported by the U.S. Air Force Office of Scientific Research Grant AFOSR-86-0159.

References

[1]Francis, M. S., Keesee, J. E., Lang, J.D., Sparks, G.W., and Sisson, G.E., "Aerodynamic Characteristics of an Unsteady Separated Flow," *AIAA Journal*, Vol. 17, Dec. 1979, pp. 1332–1339.

[2]Luttges, M. W., Robinson, M. C., and Kennedy, D. A., "Control of Unsteady Separated Flow Structures on Airfoils," AIAA Paper 85-0531, March 1985.

[3]Reisenthel, P. H., Nagib, H. M., and Koga, D. J., "Control of Separated Flows Using Forced Unsteadiness," AIAA Paper 85-0556, March 1985.

[4]Walker, J. M., and Chou, D. C., "Forced Unsteady Vortex Flows Driven by Pitching Airfoils," AIAA Paper 87-1331, June 1987.

[5]Consigny, H., Gravelle, A., and Molinaro, R., "Aerodynamic Characteristics of a Two-Dimensional Moving Spoiler in Subsonic and Transonic Flow," *Journal of Aircraft,* Vol. 21, Sept. 1984, pp. 687–693.

[6]Costes, M., Gravelle, A., Philippe, J.J., Vogel, S., and Triebstein, H., "Investigation of Unsteady Subsonic Spoiler and Flap Aerodynamics," *Journal of Aircraft,* Vol. 24, Sept. 1987, pp. 629–637.

[7]Viets, H., Piatt, M., and Ball, M., "Forced Vortices Near a Wall," AIAA Paper 81-0256, Jan. 1981.

[8]Huyer, S. A., and Luttges, M.W., "Unsteady Separated Flows Driven By Periodic Leading-Edge Deformation," AIAA Paper 87-1234, June 1987.

[9]Koga, D. J., "Control of Separated Flowfields Using Forced Unsteadiness," Ph.D. Thesis, Illinois Inst. of Technology, Chicago, IL, Dec. 1983.

[10]Nagib, H. M., Reisenthel, P. H., and Koga, D. J., "On the Dynamical Scaling of Forced Unsteady Flows," AIAA Paper 85-0553, March 1985.

[11]Ahmed, S., and Hancock, G. J., "On The Local Flow About a Spoiler Undergoing Transient Motion at Subsonic Speeds," Queen Mary College, London, QMC/EP-1050, June 1983 (available through NTIS as PB88-105291).

[12]Bearman, P. W., Graham, J. M. R., and Kalkanis, P., "Numerical Simulation of Separated Flow Due to Spoiler Deployment," *The Prediction and Exploitation of Separated Flow,* Royal Aeronautical Society, April 1989, pp. 2.1–2.15.

[13]Koga, D. J., Nelson, C. F., and Eaton, J. K., "A New Program for Active Control of Unsteady, Separated Flow Structures," *Workshop II on Unsteady Separated Flow—Proceedings,* " U.S. Air Force Academy, Colorado Springs, CO, FJSRL-TR-88-0004, Sept. 1988, pp. 343–347, (available through NTIS as AD-A202 021).

[14]Ghia, U., Zuo, L., and Ghia, K.N., "Analysis and Control of Unsteady Separated Flows," AIAA Paper 89-1018, March 1989.

[15]Adams, E. W., and Eaton, J. K., "An LDA Study of the Backward-Facing Step Flow, Including the Effects of Velocity Bias," *Journal of Fluids Engineering,* Vol. 110, No. 3, Sept. 1988, pp. 275–282.

[16]de Brederode, V.A.S.L., and Bradshaw, P., "Three-Dimensional Flow in Nominally Two-Dimensional Separation Bubbles, I. Flow Behind a Rearward-Facing Step," Imperial College, London, I.C. Aero Rept. 72–19, 1972.

[17]Bendat, J. S., and Piersol, A. G., *Random Data: Analysis and Measurement Procedures,* 2nd ed., Wiley-Interscience, New York, 1986, pp. 74–88.

[18]Moffatt, R. J., "Contributions to the Theory of Single-Sample Uncertainty Analysis," *Journal of Fluids Engineering,* Vol. 104, No. 2, June 1982, pp. 250–260.

[19]Reynolds, W. C., and Carr, L. W., "Review of Unsteady, Driven, Separated Flows," AIAA Paper 85-0527, March 1985.

[20]Hinze, J. O., *Turbulence,* 2nd ed., McGraw-Hill, New York, 1975, pp. 771–774.

[21]Brereton, G. J., and Reynolds, W. C., "Experimental Study of the Fluid Mechanics of Unsteady Turbulent Boundary Layers," Dept. of Mechanical Engineering, Stanford Univ., Stanford, CA, May 1987, pp. 213–215 (available through NTIS as AD-A184 856).